Size, density and composition of cell–mineral aggregates formed during anoxygenic phototrophic Fe(II) oxidation: Impact on modern and ancient environments

Nicole R. Posth [a,*], Sonia Huelin [a], Kurt O. Konhauser [b], Andreas Kappler [a]

[a] Geomicrobiology, Center for Applied Geosciences, University of Tuebingen, Sigwartstrasse 10, 72076 Tuebingen, Germany
[b] Department of Earth and Atmospheric Sciences, University of Alberta, Edmonton, AB, Canada T6G 2E3

Abstract

Cell–Fe(III) mineral aggregates produced by anoxygenic Fe(II)-oxidizing photoautotrophic microorganisms (photoferrotrophs) may be influential in the modern Fe cycle and were likely an integral part of ancient biogeochemical cycles on early Earth. While studies have focused on the environmental conditions under which modern photoferrotrophs grow and the kinetics, physiology and mechanism of Fe(II) oxidation, no systematic analyses of the physico-chemical characteristics of those aggregates, such as shape, size, density and chemical composition, have as yet been conducted. Herein, experimental results show most aggregates are bulbous or ragged in shape, with an average particle size of 10–40 μm, and densities that typically range between 2.0 and 2.4 g/cm^3; the cell fraction of the aggregates increased and their density decreased with initial Fe(II) concentration. The mineralogy of the ferric iron phase depended on the composition of the medium: goethite formed in cultures grown by oxidation of dissolved Fe(II) medium in the presence of low phosphate concentrations, while poorly ordered ferrihydrite (or Fe(III) phosphates) formed when amorphous Fe(II) minerals (Fe(II)-phosphates) and high concentrations of phosphate were initially present. Importantly, in all experiments, a fraction of the photoautotrophic cells remained planktonic, demonstrating a constant stoichiometric excess of Fe(III) compared to the autotrophically fixed carbon in the biogenic precipitate. These results not only have an important bearing on nutrient and trace element cycling in the modern water column, but the size, shape and composition of the aggregates can be used to estimate aggregate reactivity during sediment diagenesis over short and geologic time scales.

1. INTRODUCTION

Anoxygenic Fe(II)-oxidizing photoautotrophic bacteria are found in a variety of oxygen-poor freshwater and marine settings with elevated Fe(II) concentrations. The seven known strains of these organisms comprise three major photosynthetic branches; purple sulfur, purple non-sulfur, and green sulfur bacteria (Widdel et al., 1993; Heising et al., 1999), which utilize light energy to oxidize Fe(II) and reduce CO_2, forming Fe(III) oxides and biomass in the following process:

$$4Fe^{2+} + HCO_3^- + 10H_2O \rightarrow 4Fe(OH)_3 + CH_2O + 7H^+ \qquad (1)$$
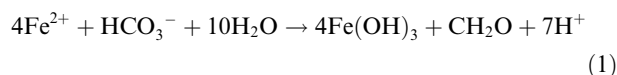
Aside from dissolved Fe(II), anaerobic Fe(II)-oxidizing phototrophs can also use a diverse set of substrates as electron donors, such as H_2, acetate, FeS and $FeCO_3$ (Kappler and Newman, 2004).

Since the isolation of these modern strains, increased knowledge of their diverse habitats, physiology, as well as the rates and magnitude at which they oxidize Fe(II), supports their potential as important players in the global iron

* Corresponding author. Tel.: +49 7071 29 73184; fax: +49 7071 29 5059.
  E-mail address: nicole.posth@uni-tuebingen.de (N.R. Posth).

cycle (Thamdrup, 2000; Kappler and Straub, 2005; Weber et al., 2006; Hegler et al., 2008). For example, the formation of reactive Fe(III) compounds is promoted by bacterial Fe(II) oxidation, forming an integral part of the Fe cycle at oxic–anoxic interfaces (Sobolev and Roden, 2001). In addition, the importance of anoxygenic Fe(II)-oxidizing phototrophs for ancient biogeochemical cycles was hypothesized several decades ago (e.g., Garrels et al., 1973; Hartman, 1984), yet such strains have only been successfully isolated within the past 15 years (Widdel et al., 1993). Recent genetic studies suggest Fe(II)-oxidizing phototrophs as the forerunners of oxygenic photosynthesis (Brocks et al., 2005; Papineau et al., 2005; Xiong, 2006; Rashby et al., 2007). Due to their oxygen-free, light-driven metabolism, they are also presumed to be involved and in the precipitation of Precambrian banded iron formations (Konhauser et al., 2002; Kappler et al., 2005a; Trouwborst et al., 2007; Posth et al., 2008; Posth et al., in press).

The mechanism behind Fe(II) oxidation in phototrophic bacteria is still not fully understood. Initial studies postulated that Fe(II) oxidation must be located at the cell surface; if it were to take place in the periplasm or cytoplasm, the massive amounts of poorly soluble Fe(III) oxides formed would impede cell function (Ehrenreich and Widdel, 1994). Therefore, theoretical models place a redox-active component at the outer cell membrane with electrons transported through the periplasm to the reaction center; a similar mechanism has been put forth for acidophilic Fe(II)-oxidizing bacteria *Acidithiobacillus ferrooxidans* (Yarzábal et al., 2002). More recently, however, the operons responsible for phototrophic Fe(II) oxidation in two strains were identified, one part of which in both strains encode c-type cytochromes, which could function as the Fe(II) oxidoreductase (Croal et al., 2007; Jiao and Newman, 2007). This suggests that Fe(II) oxidation may take place there, thus requiring some mechanism which prevents inner-cellular precipitation of ferric iron. Such mechanisms could be the production of a pH microenvironment around the cell which would allow for Fe(III) oxide precipitation away from the cell wall, solubilization of the Fe(III) by complexation, or possibly surface charge modification (Sobolev and Roden, 2001; Kappler and Newman, 2004; Schädler et al., 2009).

For Fe-rich systems, the nature of the Fe(III) mineral–cell aggregates formed from this metabolism are of fundamental importance to the reactions in these settings. It is known that biogenic Fe(III) mineral–cell aggregates are reactive, sometimes more so than their abiogenic counterparts (James and Ferris, 2004; Roden, 2004). Mineralogical studies with Fe(II)-oxidizing phototrophs show that unlike the nitrate-reducing Fe(II)-oxidizing strain *Acidovorax* sp. BoFeN1 (Kappler et al., 2005b), precipitates are associated with the cell wall, but do not cover them completely. Indeed, STXM studies have shown that the Fe(III) minerals precipitate exclusively extracellularly on polymer fibers emerging from the cells, which are coated with Fe(III) concentrations that decreases with distance from the cell (Miot et al., 2009). This suggests that the Fe(III) is released in dissolved form as an inorganic aqueous complex or colloidal aggregate prior to mineral precipitation (Kappler and New-

man, 2004). This differs from similar studies with the encrusting nitrate-reducing Fe(II)-oxidizing strain *Acidovorax* BoFeN1, for which STXM studies found a 40-nm thick mineralized layer within the periplasm (Miot et al., 2009).

Importantly, cell–Fe(III) aggregates produced by aerobic or anaerobic Fe(II)-oxidizing bacteria will settle out of the water column to accumulate in the bottom sediment. Once buried, these aggregates comprise a highly reactive fraction of sediment that will influence the early stages of diagenesis and determine the course of mineral transformations over the long term. For example, Fe(III) oxyhydroxide particles have a high specific surface area which makes them ideal sorbents for a number of major and trace solutes (Fortin et al., 1993; Clarke et al., 1997). Consequently, the transport and mobility of various ions, metal complexes and pollutants (i.e., As, Cu) in modern Fe-rich surface water and aquifer systems is greatly impacted by the composition and character of the minerals in sediment. Studies with abiotically produced minerals established that iron minerals with different crystal sizes vary significantly in surface area (ferrihydrite ranges between 250 and 350 m^2/g (Cornell and Schwertmann, 2003) and therefore in stability, solubility and reactivity (Schwertmann and Cornell, 2000). With their organic carbon component, biogenic minerals, such as the aggregates produced by Fe(II)-oxidizing phototrophs, may be particularly reactive in Fe-rich settings.

While it is evident that microbial Fe(II) oxidation represents an important link in the global Fe cycle, the study of these strains and their mineral products is still nascent. The microbial and geochemical complexity of natural settings makes full understanding of the role of cell–mineral aggregates produced by Fe(II)-oxidizing phototrophs in an environmental system challenging. For instance, it is unclear how the cell (organic carbon) component in the aggregate influences the mineral properties and thus the interactions of the iron minerals with nutrients, contaminants, and other ions in solution. Therefore, in this study, cell–Fe aggregates from pure lab strains were classified by size, morphology, density and composition in order to estimate the impact of cell–mineral aggregates in both modern and ancient systems. Aggregate behavior, such as sedimentation rate, is also calculated for marine and freshwater systems in an attempt to tie processes of Fe(II) oxidation in the surface water column to diagenetic recycling in the bottom sediment.

2. MATERIALS AND METHODS

2.1. Source of the microorganisms

Rhodobacter ferrooxidans sp. strain SW2 was isolated from a pond in Schaumburger Wald, Hannover region, Germany (Ehrenreich and Widdel, 1994). *Chlorobium ferrooxidans* sp. strain KoFox (in co-culture with *Geospirillum* sp. strain KoFum) was isolated from a ditch near the University of Konstanz, Germany (Heising et al., 1999). *Thiodictyon* sp. strain F4 was isolated from a freshwater marsh in Woods Hole, MA (Croal et al., 2004). All three strains have been maintained in our lab strain collection for the past several years.

2.2. Preparation of the growth medium and cultivation conditions

A 10-fold freshwater medium stock solution was prepared and added to distilled water to yield a final concentration in the medium of 0.5 g/l $MgSO_4 \cdot 7H_2O$, 0.6 g/l KH_2PO_4, 0.3 g/l NH_4Cl, and 0.1 g/l $CaCl_2 \cdot 2H_2O$. This growth medium was autoclaved in a Widdel flask. After autoclaving, the medium was cooled to room temperature under a N_2/CO_2 atmosphere (90:10). Finally, the following components were added in the order listed: bicarbonate buffer solution ($NaHCO_3$) to a 22 mM final concentration in the medium, 1 ml/l trace element solution SL10, 1 ml/l Selenite–Tungsten solution (after Widdel, 1980), 1 ml/l of a 7-vitamin solution (Widdel and Pfennig, 1981). After pH-adjustment to pH 6.9, 25 ml of medium were filled into 58-ml serum bottles, closed with butyl-rubber stoppers, crimped, and the headspace was flushed with N_2/CO_2 (90:10). The Fe(II) (either 4 or 10 mM final concentration) was added directly into the serum bottles from a 1 M stock solution of $FeCl_2 \cdot 4H_2O$, resulting in an unfiltered medium containing Fe(II) precipitates from the added Fe(II) plus the bicarbonate and phosphate in the medium. Filtered medium was prepared in parallel in order to grow cultures with only a dissolved Fe(II) source. Here, after the addition of Fe(II) from the 1 M stock solution of $FeCl_2$, the medium was filtered with a 0.2 μm filter in a glove box (100% N_2) and transferred into serum bottles, also resulting in lower phosphate concentrations in the final culture medium (see also Kappler and Newman, 2004). In case of growth with H_2 as electron donor, the headspace was exchanged with overpressure of H_2/CO_2 (90:10) every 2 days.

Cultures of *R. ferrooxidans* sp. strain SW2, *Thiodictyon* sp. F4 and *C. ferrooxidans* sp. strain KoFox were inoculated with 2% inoculum from cultures pre-grown on H_2/CO_2 or iron and incubated at 21 °C at light intensity equal or higher than 700 lux. All cultures were set-up in triplicate for each strain and for each Fe(II) concentration. Control samples contained all medium components besides the bacteria.

2.3. Preparation of iron (oxy)hydroxides

Suspensions (0.5 M) of four different iron oxides, hydroxides and oxyhydroxides, (ferrihydrite ($Fe_5HO_8 \cdot 4H_2O$), goethite (α-FeOOH), magnetite (Fe_3O_4) and lepidocrocite (γ-FeOOH)), were prepared in distilled water. All iron oxides, except for ferrihydrite, were supplied by Bayferrox (LANXESS Inorganic Pigments, Krefeld, Germany). For the synthesis of 2-line ferrihydrite, 40 g $Fe(NO_3) \cdot 9H_2O$ were dissolved in 500 ml Millipore water and 310 ml of 1 M KOH was added at a fixed addition rate of 100 ml/min, while vigorously stirring with a magnetic stirrer. After the pH was adjusted to ~7.5 by the addition of 1 M KOH, the suspension was left on the shaker for approximately 12 h. The pH was then measured and re-adjusted to pH 7.5 when found necessary. The mineral suspension was washed 3 times with Millipore water in order to remove remnant salts. For a 0.5 M suspension, the ferrihydrite was resuspended in Millipore water. Finally, the identity of the purchased iron minerals, as well as the chemically synthesized ferrihydrite was ascertained by μ-XRD (Mineralogy, University of Tuebingen).

2.4. Preparation of samples for scanning electron microscopy (SEM)

Samples were prepared as described in Schädler et al. (2008) both with and without fixation of the cells. In samples in which no fixation was carried out, approximately 1 ml of the sample was withdrawn with a syringe (in the glove box for anoxic samples) and transferred onto carbon-coated copper grids (200 mesh, holey C-coated, SPI supplies 3620C-MB). After they were dried in an anoxic chamber by exposure to the nitrogen atmosphere and no vacuum or heat, they were taken to the SEM for imaging. No further sample preparation or fixation steps were carried out in order to preserve the chemistry of the samples and in order to hinder oxidation of any remaining Fe(II). The samples were placed on aluminum stubs for imaging.

For fixation of cell–mineral aggregates, 2 ml of sample was taken from the culture bottles at the end of Fe(II) oxidation, fixed with 200 μl Karnovsky solution (para formaldehyde–glutaraldehyde mixture), dehydrated in successive isopropanol steps and transferred onto carbon-coated copper grids (200 mesh, holey C-coated, SPI supplies 3620C-MB) (for details, see Schädler et al., 2008). Gold or palladium coating was used for imaging.

2.5. Cell–mineral aggregate sample preparation for density determination

For the preparation of the samples for cell–mineral aggregate density determination, precipitates of 25-ml samples of *R. ferrooxidans* sp. strain SW2 and *Thiodictyon* sp. F4, grown either with 4 or 10 mM Fe(II), were collected stepwise by centrifugation in 1.5-ml Eppendorf tubes (14,000 rpm, 2 min; removal of the supernatant after each centrifugation step). After collecting the precipitates, they were washed 3 times with 2 ml sodium chloride (0.9%). Although we were aware of the fact that centrifugation brings with it the risk of artificial aggregation, collection of precipitate without centrifugation did not yield enough material to carry out the density experiments within a reasonable time frame.

2.6. Analytical methods

2.6.1. Fe determination

Fe(II) and Fe(III) concentrations were determined spectrophotometrically (FlashScan 550, Analytik Jena, Germany) via the ferrozine method (after Viollier et al., 2000). Samples were prepared in triplicate with a blank, which allowed determination of Fe(II) loss due to sorption to the glass culture bottle or potential abiotic oxidation. Samples of the Fe(II)-grown cultures were taken sterilely with a syringe through the butyl-rubber culture bottle stopper, diluted and prepared for Fe(II) and total Fe determination as further described in Hegler et al. (2008). The oxidation rates of the triplicates were averaged and the standard deviation calculated.

2.6.2. Determination of aggregate biomass composition

The determination of biomass in the suspension at the end of Fe(II) oxidation was carried out via cell counts (following Lovley and Phillips, 1986; Suter et al., 1988; Roden and Zachara, 1996). Cell counts were performed for the culture solution directly after inoculation of the strains and at the end of Fe(II) oxidation. For all experiments, cultures were grown in triplicate, with an abiotic (uninoculated) blank. 0.5–8 ml of sample was taken sterilely with syringe through the butyl-rubber stopper of the culture tubes and transferred into a test tube. The sample was immediately fixed with 100 μl of 25% glutaraldehyde and 8.9 ml oxalate solution (28 g ammonium oxalate and 15 g oxalic acid/1 l Millipore water) added. Then, one ml of a filtered, anoxic 100 mM ferrous ethylene-diammonium sulfate was added to each test tube. The tubes were swirled periodically for 10 min until all of the Fe mineral particles were dissolved. Fifty-five microliters of DAPI (4′,6-diamidino-2-phenylindole-dihydrochloride) solution was added to each test tube in order to reach the optimum staining concentration of 10 mg/l. After 5 min, 1–3 ml (depending on cell number) was then transferred to a filter and viewed with fluorescence (AxioVison Microscope, Zeiss) and an oil immersion object lens.

2.6.3. Scanning electron microscopy

For imaging via scanning electron microscopy, the samples were analyzed with a Field Emission Scanning Electron Microscope (Leo 1550 VP) at the Natural and Medical Science Institute in Reutlingen (NMI) and with a Scanning Electron Microscope (Leo 1450 VP) at the University of Tuebingen, Institute for Geoscience, following methods described in Schädler et al. (2008). At the NMI, an in-lens detector was used for imaging. The acceleration was 2 kV and the working distance was 3 mm. During microscopy, the samples were exposed to air for a maximum of 30 s from the opening of the glass until the pump in the microscope chamber was started. At the University of Tuebingen, the secondary electron (SE) imaging was carried out at an acceleration of 15–20 kV. The working distance was 5–12 mm and pressure targeted to 8×10^{-6} mbar. The samples were sputter-coated (Sputter Coater BAL-TEC Model SCD 005/CEA 035) with Au for 150 s to achieve a 45 nm gold coverage thickness.

2.6.4. Laser light diffractometry

Laser diffractometry (particle size analyzer Malvern Mastersizer Micro, Malvern, UK) was used for cell–mineral aggregate size determination. The samples were added stepwise as slurry to distilled water at a constant stirring rate of 1490 rpm (which allowed suspension of all the material without causing air entrainment) directly from the bottles until a grade of obscuration of approximately 15% was achieved. A depiction of three subsequent runs (Fig. A1) demonstrates that mechanical disintegration of the particles due to the stirring is no longer significant after the first run. All data for particle size via this method is presented as an average of three runs, with bars depicting the error.

2.6.5. Mineral analysis by μ-X-ray diffraction (μ-XRD)

Biogenic minerals were withdrawn in an anoxic glove box with a syringe. In order to increase the sample amount for μ-XRD analysis, 10 ml of samples with a 4 mM Fe(II) concentration and 8 ml of those with 10 mM Fe(II) were transferred stepwise into 2 ml plastic tubes. These were centrifuged at 12,000 rpm for 2 min in between each step, followed by removal of the supernatant. After the last step, the precipitates were washed 3 times in an anoxic glove box with 1.5 ml of anoxic water to remove loosely sorbed Fe(II) from the precipitates and to avoid the oxidation and formation of non-biogenic Fe(III) precipitates. The tubes were then left open in the anoxic chamber for 24 hours until the precipitates were dried.

The dried precipitates were ground in a mortar in the glove box and 40–60 μl of ethanol were added in order to have a suspension that could be transferred with a glass pipette onto a silicon wafer sample holder. After the ethanol evaporated, the sample holder was covered with a piece of transparent plastic foil in order to prevent oxidation of potentially present Fe(II) species or Fe(II) mineral phases, and transported in a tightly closed (air-tight) glass container to the μ-XRD instrument for measurement. They were then quickly placed in the μ-XRD and the measurements were performed within 2 min in order to prevent significant oxidation of oxygen-sensitive mineral phases. This method was designed by Katja Amstaetter and Christoph Berthold at the University of Tuebingen.

2.6.6. Mössbauer spectroscopy

The minerals produced both in filtered (only dissolved Fe(II)) and non-filtered medium were studied using Mössbauer spectroscopy. The cell–mineral aggregates were separated from solution by centrifugation (10 min, 6500g) and the supernatant was removed in a glove box (100% N$_2$). These aggregates including the Fe minerals were then allowed to dry in an anoxic chamber. Before removal from the anoxic chamber, the solid samples were placed between two layers of Kapton® tape. Mössbauer spectra were collected with a constant acceleration drive system in transmission mode and with a ^{57}Co source at room temperature. Samples were then mounted in a Janis close-cycle exchange gas cryostat, which allowed cooling of the sample to 4.2 K. Spectra were calibrated against a spectrum of α-Fe metal foil collected at room temperature. Finally, spectra calibration and fitting was carried out with Recoil® software (University of Ottawa, Canada) using Voigt based spectral lines following the model parameters of the average center shift, CS, 0.49 mm/s (CS of goethite approximately 0.48–0.5 at 4.2 K), the average quadrupole shift, ε, −0.1 mm/s (characteristic of goethite (−0.12)), the average hyperfine field, H, 48.2 T, most probable hyperfine field, H_p, was 49.3 T (goethite has a hyperfine magnetic field of about 50 T at 4.2 K).

2.6.7. Density

The density of cell–mineral aggregates and reference iron minerals was determined by following sedimentation behavior in sodium polytungstate solutions (SOMETUI, Berlin, Germany). The densities of these solutions were adjusted by addition of distilled water to a sodium polytungstate stock solution with a starting density of 3.01 g/cm^3. 0.5 ml of 500 mM suspensions of each iron (oxy)hydroxide was transferred with a 1 ml syringe to a glass test tube containing the diluted polytungstate solution.

Cell–mineral aggregate samples were added to a series of test tubes containing 10 ml of sodium polytungstate solutions at set densities of: 2.4, 2.0, 1.6 and 1.2 g/cm^3. The aggregates were allowed to settle in this solution either for 5 min or 24 h. The particles still present at the surface of the liquid had a lower or equal density than the polytungstate solution applied, while those sedimented in the tubes were those with a higher density than the solution. Those aggregates present at the surface of the solution were collected with a glass pipette and transferred into separate test tubes. The glass test tubes of either sedimented or suspended particles were then centrifuged at 7000 rpm for 10 min. After the removal and collection of the supernatant (sodium polytungstate solution) for its reuse, the precipitates (cell–mineral aggregates) were washed 3 times with 0.9% sodium chloride. Finally, the iron content of the precipitates was determined via ferrozine assay after dissolution of an aliquot in 6 M HCl (Stookey, 1970; Viollier et al., 2000).

2.7. Calculation of sedimentation rates by Stokes' Law

Following Stokes' law, particles (in our case cell–mineral aggregates), falling in a water column by their own weight, reach a terminal (settling) velocity when the frictional force combined with the buoyant force balances the gravitational force. While Stokes' law is most accurately applied for spherical particles, we have still utilized this law as an estimate of the irregular cell–mineral aggregate sedimentation rate. The resulting settling velocity (V_s) is therefore given by

$$V_s = \frac{2}{9} \frac{r^2 g (\rho_p - \rho_f)}{\eta}$$

where g = gravitational acceleration, ρ_p = particle density, ρ_f = fluid density, η = fluid viscosity, r = Stokes' radius of a particle.

3. RESULTS AND DISCUSSION

3.1. Bacterial influence on Fe mineral particles

Minerals formed by Fe metabolizing bacteria form an integral part of natural environments, but much is still unknown about the influence of the organic carbon component of cell–mineral aggregates on the mineral properties. Furthermore, it is difficult to ascertain how these aggregates interact with nutrients, contaminants, metals or ions in solution. Herein we characterized the cell–mineral aggregates formed by pure strains of anoxygenic phototrophic Fe(II)-oxidizing bacteria and found that they differ from abiogenic Fe(III) minerals in terms of morphology, mineralogy, composition, particle size, and density. A comparison of studies carried out with these strains shows that incubation time, solution chemistry and the presence of nucleation sites in the system result in changes in cell–mineral aggregate characteristics (Kappler and Newman, 2004; Posth et al., 2008; Schädler et al., 2009; Miot et al., 2009).

3.1.1. Biogenic mineral morphology and mineralogy

The cell–mineral aggregates formed by Fe(II) oxidation by anoxygenic phototrophs were ragged or bulbous, differing in morphology from chemically synthesized ferrihydrite and goethite (Fig. 1). The biogenic minerals are constructed as a network of cells and Fe(III) minerals, a C_{org}–Fe(III)–mineral system, that is characterized by large surface areas
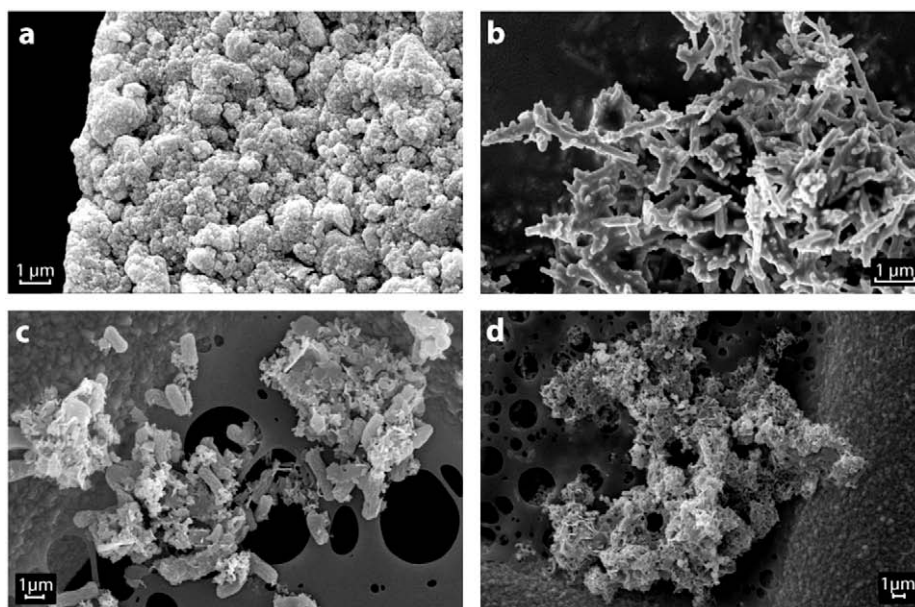

Fig. 1. Scanning electron micrographs of abiogenic and biogenic Fe minerals. (a) Chemically synthesized 2-line ferrihydrite, (b) synthetic goethite (Bayferrox, LANXESS Inorganic Pigments), (c) cell–mineral aggregates formed by *Thiodictyon* sp. strain F4 in the presence of 4 mM dissolved Fe(II) (filtered medium), (d) cell–mineral aggregates formed by *Rhodobacter ferrooxidans* sp. strain SW2 in the presence of 2 mM dissolved Fe(II) (filtered medium).

and varying surface properties within the aggregate. The C_{org}–Fe(III)–mineral components (Fig. 1), influences aggregate reactivity in microbially (as suitable electron acceptors for microbial Fe(III) reduction; Straub et al., 1998) and abiotically driven redox reactions, as well as in sorption processes (Postma, 1993; Roden and Zachara, 1996; Roden, 2003; Hansel et al., 2004; Langley et al., 2009). In the environment, the identity and reactivity of primary biogenic iron minerals are also known to change with time (Roden, 2003; Hansel et al., 2004), and be enhanced as mineral mixtures of varying crystallinity develop and mineral transformations alter surface properties (Postma, 1993). Such transformations, for example, can influence the porosity of sediment layers (e.g., Canfield, 1989) as well as biological and chemical degradation of carbon in the water column.

The biogenic Fe(III) mineral product at the end of phototrophic Fe(II) oxidation by *R. ferrooxidans* sp. strain SW2 was also strongly influenced by the bacterial growth medium composition or solution chemistry. In this study, strain SW2 cells were transferred into the batch systems from H_2-grown (Fe mineral free) cultures, ensuring that the Fe(III) mineralogy observed after Fe(II) oxidation did not stem from minerals transferred with the inoculum, but from the primary phases themselves. For one set of experiments, the medium was carbonate buffered, and contained bicarbonate along with phosphate and sulfate, as well as a variety of trace elements. $FeCl_2$ was added as an electron source (see method of medium preparation above). Past geochemical studies performed with this bacterial growth medium showed that the addition of $FeCl_2$ causes the precipitation of Fe(II)-phosphate mineral phases, mostly vivianite (Miot et al., 2009), consistent with their low solubility ($K_{sp} = 1 \times 10^{-36}$, Stumm and Morgan). Another Fe(II) mineral potentially to precipitate in this carbonate buffered medium, $FeCO_3$, is more soluble ($K_{sp} = 1 \times 10^{-10.45}$) and was not seen in the precipitate. Depending on starting Fe(II) concentration, microbial oxidation required between 3 and 12 days (Fig. A2, Hegler et al., 2008, for oxidation rates by these strains). In line with this, µ-XRD and Mössbauer spectroscopy performed at the end of Fe(II) oxidation by *R. ferrooxidans* sp. strain SW2, in medium containing high phosphate concentrations (4.4 mM), showed disordered ferrihydrite or Fe(III) phosphate (Fig. 2). The mineral product in this set-up was not seen to change its mineralogy with time nor with increased Fe concentrations (not shown). In a second set of experiments with *R. ferrooxidans* sp. strain SW2, this medium was filtered after the addition of $FeCl_2$ as a comparison. The Fe(II)-phosphate phases were largely removed by this filtration, leaving 3.6 mM dissolved Fe(II) as the electron source and lower concentrations of phosphate in solution ($\sim$40 µM, data not shown). Here, goethite, rather than disordered ferrihydrite or Fe(III) phosphate as in the non-filtered medium set-ups was detected at the end of
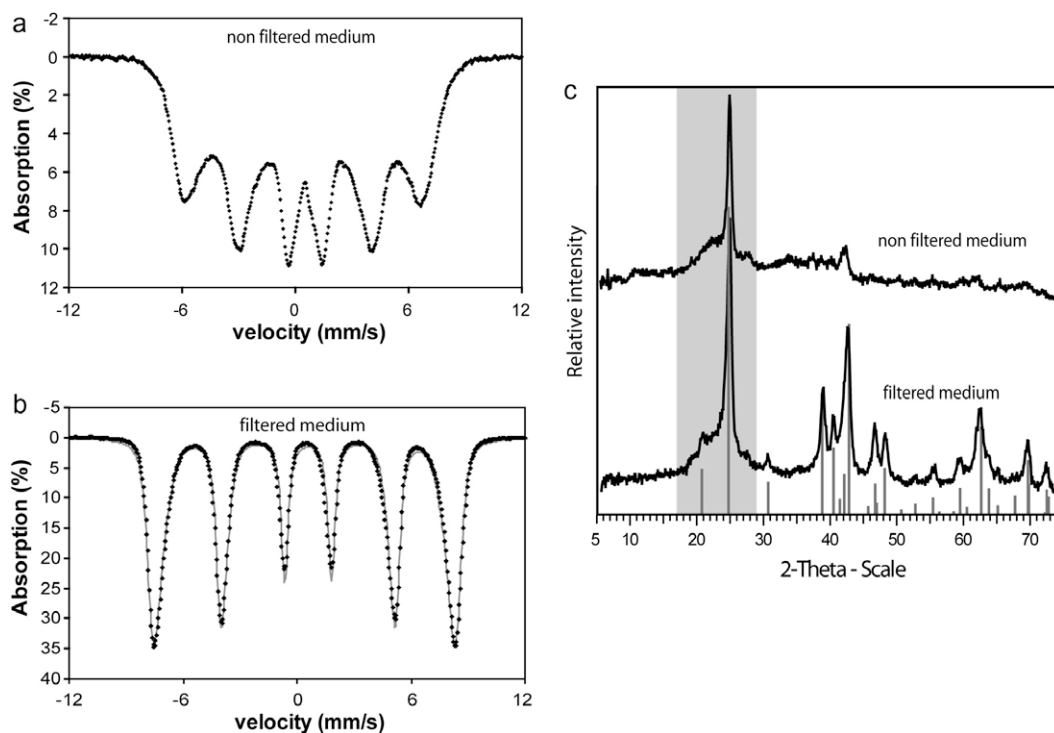

Fig. 2. Comparison of Fe(III) minerals formed during microbial Fe(II) oxidation in filtered (just dissolved Fe(II) as electron source) vs. non-filtered medium (disordered Fe(II)-phosphate is present when microbial Fe(II) oxidation starts). Mössbauer spectra of biogenic Fe(III) minerals produced by Fe(II) oxidation with *Rhodobacter ferrooxidans* sp. strain SW2 in unfiltered medium (a) and filtered medium (b). A goethite model is represented by a solid gray line. All samples were collected at 4.2 K. µ-XRD analyses of precipitates formed in filtered and non-filtered medium by strain SW2 (c). The reference pattern for goethite is shown for comparison in gray. Please note the wide gray bar which indicates the signal of the foil used to cover the sample during measurement to maintain anoxic conditions.

oxidation (Fig. 2), confirming earlier studies from our group (Kappler and Newman, 2004).

In past studies of biogenic iron minerals, the presence of pre-existing nucleation sites influenced the final mineral product. XRD studies of precipitates formed in filtered medium by the nitrate-reducing, Fe(II)-oxidizing strain *Acidovorax* sp. BoFeN1 detected the crystalline Fe(III) mineral goethite and poorly crystalline iron mineral phases. These cultures were inoculated from Fe-acetate grown cultures that contained some Fe(III) minerals in the inoculum. In cultures inoculated with cells pre-grown with only acetate (without Fe(II) and therefore also without transfer of Fe(III) phases during inoculation), poorly crystalline ferric iron (hydr)oxides were detected (Kappler et al., 2005b). The authors concluded the presence of Fe(III) nucleation sites introduced by the Fe-acetate grown inoculum aided the formation of the more crystalline goethite. The minerals formed in cultures with pre-existing Fe(III) minerals were larger and more crystalline, while in cultures without pre-existing minerals, the Fe(III) product was smaller and irregularly shaped (Kappler et al., 2005b).

While in Kappler et al. (2005b), the presence of Fe mineral nucleation sites was determined as the controlling factor for the crystallinity of the mineral product, in the present study, solution chemistry appeared to determine the primary mineral product (see also studies of passive biomineralization, Chatellier et al., 2001, 2004). The biogenic minerals produced from cultures grown in non-filtered medium were exposed to higher concentrations of phosphate (up to 4 mM), while the filtered medium contains only ~40 µM phosphate. The influence of the solution chemistry was seen in separate experiments with this medium. First, in studies of *Acidovorax* sp. strain BoFeN1 in filtered medium with an estimated initial phosphate concentration of 1.3 mM, Miot et al. (2009) observed the production of Fe(III) phosphates. Second, in experiments carried out in filtered medium with lower initial concentrations of phosphate (herein, ~40 and ~10 µM; Hohmann et al., 2010), goethite or nano-goethite were observed as main mineral products. It is well-established that abiotic primary iron mineral formation is driven by counter ions (chloride and bicarbonate) both in situ and in vitro (Konhauser, 1997; Brown et al., 1999; Schwertmann and Cornell, 2000; Chatellier et al., 2001; Fortin and Langley, 2005; also see Ferris, 2005, for a review of biogenic iron oxides). Specifically, goethite development in Fe(II) oxidation and Fe(III) mineral formation has been reported to be influenced by bicarbonate concentration in solution (Cornell and Schwertmann, 2003). For biotic systems, it is known that the presence of microbially produced Fe(II) (via microbial reduction) drives the formation of magnetite, goethite (and lepidocrocite) from ferrihydrite (Hansel et al., 2003).

By comparing the solubility of the potential end point mineral products after Fe(II) oxidation in microbial growth medium, it is expected that ferrihydrite ($K_{sp} = 1 \times 10^{-38}$, Stumm and Morgan, 1996) or even goethite ($K_{sp} = 1 \times 10^{-40}$, Cornell and Schwertmann, 2003) would form. Yet, in unfiltered medium which contains high concentrations of phosphate and carbonate (Table A1), Fe(III) phosphate ($K_{sp} = 1 \times 10^{-26}$; Stumm and Morgan, 1996) and some ferrihydrite forms rapidly and appears stable within the timeframe of these experiments (Miot et al., 2009). In filtered systems with low phosphate, the Fe(III) phosphate phase does not form after oxidation. It is likely that in unfiltered systems, the high concentrations of phosphate block the mineral surface, effectively preventing re-precipitation or transformation to goethite as is seen in filtered medium cultures. This is in contrast to the filtered medium systems of low phosphate concentrations where the ferrihydrite could transform to goethite unhindered by phosphate. As in previous studies with other Fe(II)-oxidizing bacteria and abiotic Fe(II) oxidation, geochemical parameters and environmental conditions, such as the presence of nucleation sites and solution chemistry, rather than the cell enzymatic mechanism, seem also to determine the final Fe(III) mineral phase precipitating after the initial formation of dissolved Fe(III) aquo complexes (mainly $Fe_2(OH)_2^{4+}$) (Schwertman et al., 1999) for photoautotrophic Fe (II) - oxidizing bacteria.

3.1.2. Biogenic Fe mineral composition

Anoxygenic Fe(II)-oxidizing phototrophic bacteria are loosely associated with the Fe(III) minerals they produce (Fig. 1c and d), a trait which has also been observed in natural samples (Konhauser, 1997). This differs from some phototrophic and nitrate-reducing Fe(II)-oxidizing strains, which instead become encrusted by the Fe(III) mineral product, yielding an intimate association of organic material and Fe(III) (Heising and Schink, 1998; Schädler et al., 2009). As interactions with other compounds in the environment or further transformations of the sedimented cell–mineral aggregates depend upon the surface character and composition, differences in reactivity for these two systems are expected.

It is known that an increase in initial cell number in a culture of *R. ferrooxidans* sp. strain SW2 results in a lower number of planktonic cells at the end of Fe(II) oxidation and therefore a precipitate with larger organic carbon fractions (Konhauser et al., 2005). Building on these experiments, we carried out batch experiments with *R. ferrooxidans* sp. strain SW2 to test the effect of increasing initial concentrations of Fe(II) on cell–mineral aggregate composition. Fe(II) oxidation in these experiments ran from 3 to 12 days, depending on starting Fe(II) concentration (Fig. A2). The planktonic cells and suspended Fe were quantified with respect to total cells and Fe at the end of Fe(II) oxidation. It was found that initial cell number and dissolved Fe(II) concentration in the solution influences aggregate structure. Higher initial dissolved Fe(II) concentrations in cultures resulted in a higher fraction of precipitated SW2 cells at the end of Fe(II) oxidation (Fig. 3 and Table 1), which confirms the lower density also seen in these aggregates (Fig. 4). The organic carbon fraction of the precipitate increased dramatically with initial Fe(II) concentration; from 63% in the precipitate in cultures of 0.8 mM initial dissolved Fe(II) concentration to 96% in the precipitate in 4 mM initial concentration cultures (Table 1). The
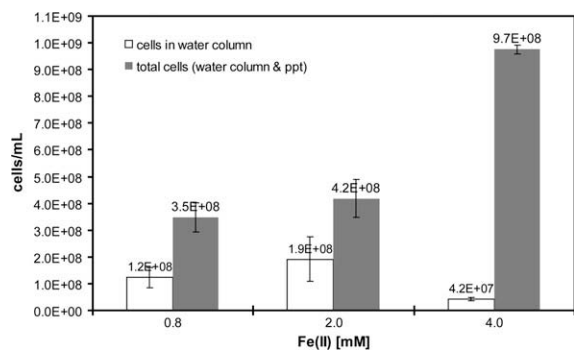
Fig. 3. Total organic carbon (water column and precipitates) and organic carbon in the water column quantified as the number of suspended microbial cells in cultures of *Rhodobacter ferrooxidans* sp. strain SW2 growing with 0.8, 2 or 4 mM Fe(II). Samples were taken directly at the end of Fe(II) oxidation.

Table 1
Percent of cells found in suspension and in the precipitated aggregate at the end of Fe(II) oxidation by the anoxygenic Fe(II)-oxidizing phototroph, *Rhodobacter ferrooxidans* sp. strain SW2. Refer to Appendix A4 for detailed description of Fe/C ratio estimation.

Fe(II) (mM)	% Cells in suspension	SD (%)	% Cells in agg/ppt	Fe/C ratio[a]
Harvested directly after completion of Fe(II) oxidation				
0.8	37	±17	63	1.80:1
2	48	±25	52	4.38:1
4	4	±3	96	2.24:1

[a] A 4:1 Fe/C ratio in the aggregates would be expected in a scenario where all Fe(III) produced by photoautotrophic Fe(II) oxidation were associated with the cell biomass produced.

Fe/C ratio in the aggregates would be 4:1 if all Fe(III) produced by photoautotrophic Fe(II) oxidation were associated completely with all cell biomass produced. In our experiments a surplus of Fe(III) was seen in the Fe:C ratio, which was between 1.80:1 and 4.38:1 (Tables 1 and A2, total organic carbon related to cell density with 50% C content in cell; Neidhardt et al., 1990). An increase in Fe:C not linearly correlated to the increase in initial Fe(II) concentration in the system. Importantly, as a consequence, a fraction of cells remained planktonic in all set-ups after the end of Fe(II) oxidation, which resulted in a constant stoichiometric excess of Fe(III) in the precipitate for all scenarios of initial cell number and Fe(II) concentration (Fig. 3).

In a scenario in which cell–mineral aggregates would settle to the sediment surface, reduction of these Fe(III) minerals during diagenesis could be instigated not only by the co-precipitated cells, but also by native Fe(III)-reducing microorganisms. Even after all the C is oxidized, there would still be Fe(III) minerals remaining, which could account for the lack of carbon found in ancient BIFs sediments. Yet, the potential consequences for a modern system can be illustrated by studies on modern systems. Roden (2003) showed the impact of the functional groups

exposed in cell–mineral aggregates for metal sorption to these particles; the increased amounts of bacterial organic matter enhanced solid-phase metal partitioning. The association between positively charged Fe(III) (hydr)oxides and negatively charged cell surfaces in the aggregate would dictate reactions with charged organic molecules, nutrients and metal ions in an aqueous environment.

3.1.3. Biogenic Fe mineral particle size

It is known that particle size and aggregation behavior, particularly of smaller primary particles, influences mineral solubility and reactivity (Cornell and Schwertmann, 2003), and in the case of ferric oxyhydroxides, determines whether Fe(III)-reducing bacteria can access these minerals. In order to compare chemically synthesized Fe(III) minerals to the biogenic Fe(III) minerals, the particle diameters of both chemically synthesized ferrihydrite and goethite were measured using light diffraction and SEM. This was then compared to the diameter of the cell–mineral aggregates formed in culture. The chemically synthesized ferrihydrite had an average hydrodynamic particle size of 8–16 μm (Fig. 5a) although primary ferrihydrite particles are on the nm scale (Fig. 1a), while the goethite (BayFerrox 910 pigment) had a peak hydrodynamic particle diameter of approximately 5 μm (Figs. 1a, b and 5a).

The cell size of the anoxygenic phototrophs, *Thiodictyon* sp. strain F4, *C. ferrooxidans* sp. strain KoFox and *R. ferrooxidans* sp. strain SW2, grown in the absence of iron (with acetate or H_2/CO_2, 10:90), can be estimated with SEM (Fig. 6). *Thiodictyon* sp. strain F4 differs from the other species in that it forms gas vacuoles, making them the largest of the anoxygenic phototrophs yet studied with a length as much as 4 μm (Fig. 6a). As a co-culture, *C. ferrooxidans* sp. strain KoFox shows cell sizes on average of 0.7 μm in length (for the phototrophic Fe(II)-oxidizer) and 10 μm in length for the chemotrophic co-culture strain KoFum (Fig. 6b). *R. ferrooxidans* sp. strain SW2 cultures contained cells approximately 1 μm in length and 0.5 μm in width (Fig. 6c).

The anoxygenic Fe(II)-oxidizing phototrophs formed cell–Fe mineral aggregates across a wide size range for all Fe(II) concentrations tested (Table 2) as based on SEM (Fig. A3) in contrast to the values based on hydrodynamic size (Fig 5). These aggregates have an average particle size of 10–40 μm, with some aggregates reaching ~56 μm in diameter (Fig. 5b and Table 2). While aggregate sizes were similar for strain SW2 and F4, the aggregates produced by *C. ferrooxidans* sp. strain KoFox were slightly larger (Table 2 and Fig. A3) with aggregates of up to 56 μm at 2 mM initial Fe(II) concentrations (Table 2). EM images showed that on average, strain F4 builds larger aggregates in the presence of Fe than strain SW2 (Table 2); a trait not detected with laser light diffraction. While a strong trend between initial Fe(II) concentration and aggregate size was not observed, large aggregates were no longer observed on average in cultures of high Fe(II) concentrations (e.g., 10 mM initial dissolved Fe(II)) (Table 2 and Fig. A3). It is plausible that cells and Fe(III) oxides form mineral nets which grow larger in size. At higher Fe(II) concentrations,
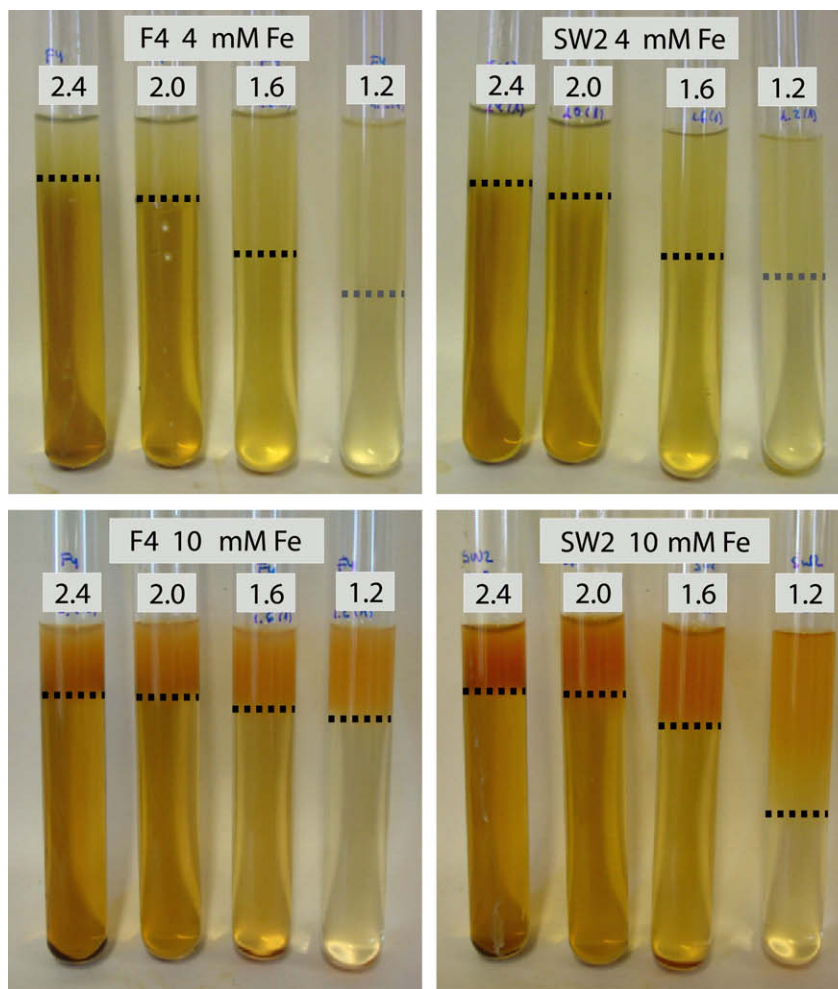
Fig. 4. Density of cell–mineral aggregates formed by two different photoautotrophic Fe(II)-oxidizing strains with two concentrations of Fe(II) as determined by observing sedimentation behavior in sodium polytungstate solution. Samples of *Thiodictyon* sp. strain F4 and *Rhodobacter ferrooxidans* sp. strain SW2 cultured in the presence of either 4 or 10 mM Fe(II) were collected stepwise and centrifuged. 0.5 ml of 500 mM suspensions were added to four solutions of sodium polytungstate with densities of 2.4, 2.0, 1.6 and 1.2 g/cm^3. Images were taken after 5 min. Particles with a higher density than the solution precipitate settled to the bottom, while those less dense or of equal density remain at or near the surface of the solution. Dashed lines indicate precipitate fronts in the solution.

the higher production of Fe(III) oxides may cause the relative stability of larger aggregates to break causing the resilience of these large aggregates to fail, yielding smaller aggregates than at lower concentrations. In co-cultures of KoFox, the chemolithotroph, KoFum, which can exceed lengths of 10 μm (Fig. 6b) could help establish these large cell–mineral aggregates, especially in fairly fresh cultures with vital chemolithotrophs. The controlling factor in the size of cell–mineral aggregates, therefore, seems not to be initial Fe(II) concentration, but rather cell characteristics, like size and surface properties.

3.1.4. Biogenic Fe mineral density

As a comparison, the density of chemically synthesized goethite, ferrihydrite, as well as magnetite (Bayoxide E8710) and lepidocrocite (Bayferrox 943) was first estimated by precipitation in a polytungstate solution set at

3.01 g/cm^3. As sedimentation was observed within 48 h for all minerals in this solution, particle densities were higher than 3.01 g/cm^3 (Fig. A4). This is consistent with past iron mineral density determination of goethite (4.26 g/cm^3), ferrihydrite (3.96 g/cm^3), magnetite (5.18 g/cm^3) and lepidocrocite (4.08 g/cm^3) (Schwertmann and Cornell, 2000).

Of the iron minerals tested, magnetite precipitated fastest, attributable to its higher density (Fig. A4). In fact, in previous studies on the settling behavior of iron oxide suspensions, magnetic flocs (maghemite) were found to be on average 1.3–1.4 times denser than their non-magnetic analogs (hematite), driven by magnetic forces between the particles (Glasrud et al., 1993). In comparison to magnetite where complete sedimentation was observed already after 24 h, a fraction of ferrihydrite, goethite and lepidocrocite with smaller particle size remained in suspension after a
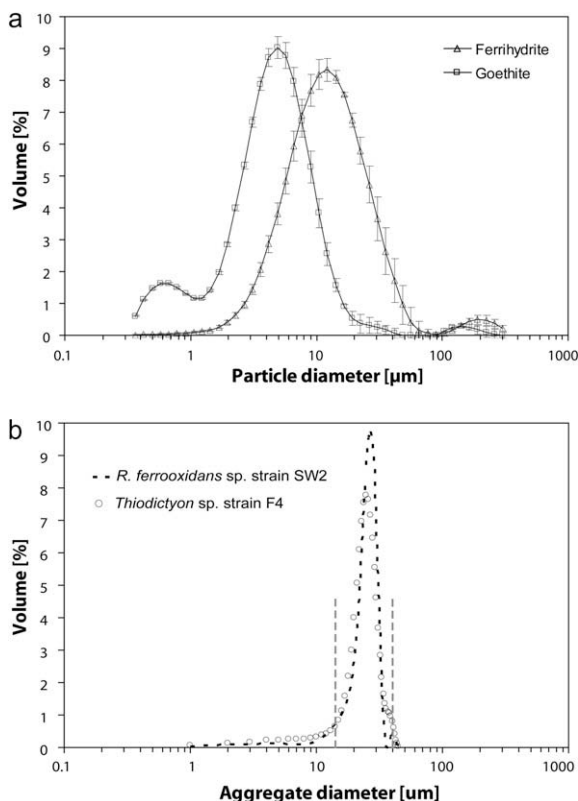
Fig. 5. Hydrodynamic particle size distribution of chemically synthesized ferrihydrite and goethite (a). In (b), cell–mineral aggregates formed by oxidation of 4 mM Fe(II) by the photo-trophic Fe(II)-oxidizers *Thiodictyon* sp. F4 and *Rhodobacter ferrooxidans* sp. strain SW2 were measured in three successive laser diffractometry runs (average of all three measurements shown). Dashed gray lines (–) represent the aggregate diameter range of the biogenic minerals.
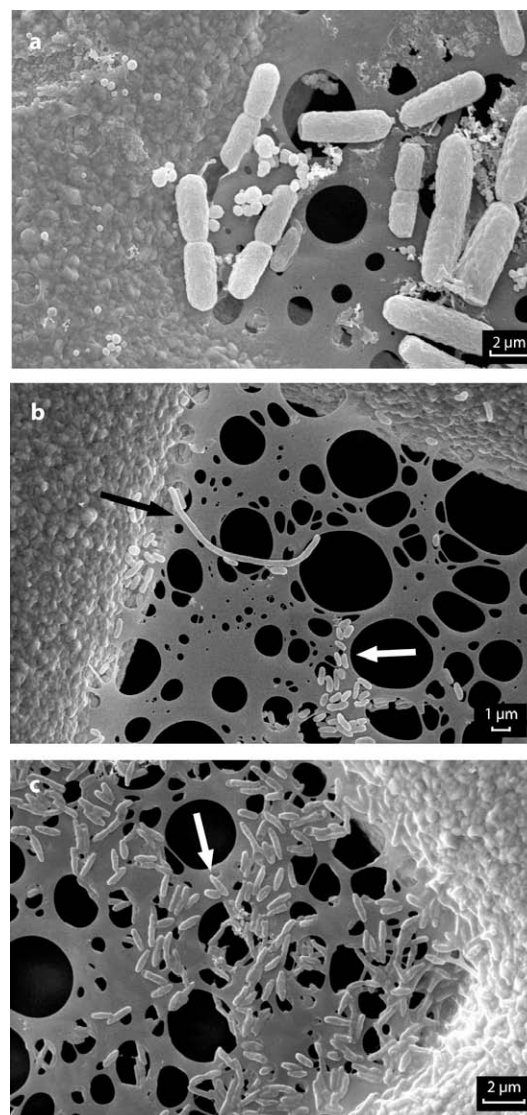

Fig. 6. Scanning electron micrographs (SEM) depicting cell morphology. (a) *Thiodictyon* sp. F4 grown on 10 mM acetate. Any Fe(III) minerals seen in the image were transferred with the inoculum. (b) *Chlorobium ferrooxidans* sp. strain KoFox (white arrow) grown with H_2/CO_2 (90:10). The large, chemolithic strain, KoFum, grows in co-culture with the phototroph (black arrow). (c) *Rhodobacter ferrooxidans* sp. strain SW2 (white arrow), grown with H_2/CO_2 (90:10).

24 h period (Fig. A4). Considering the 10 ml volume of polytungstate solution in the culture tubes and the particle densities suggested by Schwertman and Cornell (2000), applying Stokes' law predicts the size of these particles would be less than 0.5 μm in diameter (for goethite <0.412 μm and for lepidocrocite <0.446 μm). Such particles may be visible in these samples as the appendices along the goethite needles (Fig. 1b).

From the biogenic Fe(III) precipitates, aggregates formed by *R. ferrooxidans* strain SW2 and *Thiodictyon* sp. strain F4 were chosen for density studies (Fig. 4). As these cells differ greatly in size (Fig. 6) and one of them contains gas vacuoles, it was believed that density could differ with amount of biomass in the aggregates and therefore with initial Fe(II) concentration. For both 4 mM and 10 mM initial Fe(II) concentration, it was found that the biogenic minerals formed by both strain SW2 and strain F4 had densities between 2.0 and 2.4 g/cm^3 with only a small fraction at higher values (Fig. 4). As the biogenic Fe minerals formed by the anoxygenic phototrophs contain an organic carbon fraction (cells), it was not surprising to find that the densities of these particles were lower than abiotically formed Fe

minerals (Fig. 4). Both strains SW2 and F4 formed cell–mineral aggregates with very similar densities, which only deviated at high initial Fe(II) concentrations. At 10 mM initial dissolved Fe(II) concentrations, cell–mineral aggregates produced by strain SW2 settled faster than those formed by strain F4. The faster settling of SW2 cell–mineral aggregates may be due to the size or the gas vacuoles of *Thiodictyon* sp. strain F4. These vacuoles may help the strain remain buoyant in a water column. The cell–mineral aggregates formed by the smaller strain SW2 are denser without the vacuoles and subsequently dragged out of suspension.

Table 2

The size of cell–mineral aggregates based on SEM produced by *Thiodictyon* sp. strain F4, *Rhodobacter ferrooxidans* sp. strain SW2 and *Chlorobium ferrooxidans* sp. strain KoFox by the oxidation of initial concentrations of 2, 4 and 10 mM Fe(II).

Fe(II) in medium (mM)	Aggregate size range (μm)	Mean (μm)	Median (μm)
Cell–mineral aggregates formed by Thiodictyon sp. F4			
2	5–40	16.8	14.0
4	2–52	16.3	11.5
10	2–32	10.4	7.9
Cell–mineral aggregates formed by Rhodobacter ferrooxidans sp. strain SW2			
2	3–28	11.2	9.5
4	3–12	6.7	6.0
10	2.5–35	12.5	8.3
Cell–mineral aggregates formed by Chlorobium ferrooxidans sp. strain KoFox			
2	5–56	27.2	25.0
4	5–45	18.3	17.0
10	2–20	7.8	6.5

In general, aggregates from cultures grown with high initial Fe(II) concentrations settled slower than those grown at lower Fe(II) concentrations (Fig. 4). On the one hand, cultures grown with high initial Fe(II) concentrations produced on average aggregates of smaller particle size (see above). Furthermore, in cultures containing higher concentrations of Fe, the aggregate Fe:C ratio shifts as more cells are produced and "trapped" in the aggregates (see above). A higher organic carbon component would lower the density of the aggregates overall and increase settling time.

3.2. Sedimentation and water column residence time of cell–mineral aggregates

The particle size and density measurements made for abiotically formed ferrihydrite, anoxygenic phototrophic cells grown without Fe, and biogenic Fe minerals can be used to estimate sedimentation rates (or residence time in a water column) by applying Stokes' Law. In general, sedimentation rate increases with particles size (Fig. 7), and cells alone settle slower than pure Fe minerals. The cell component of the biogenic minerals lowers the total particle density resulting in a decreased sedimentation rate. In seawater, biogenic minerals would settle at a rate of 0.42–10.6 m/h on average (Fig. 7a). The spread between sedimentation rates was highest between large cell particles and cell–Fe mineral aggregates. In seawater settings, the effect of higher fluid viscosity and density, as considered by Stokes' law, shows that sedimentation rates decreased slightly as compared to a freshwater system (Fig. 7b). For example, in a freshwater setting, a cell–mineral aggregate of the average 20 μm size would require 1.11 days to fall through 100 m. In a seawater setting, this aggregate would settle out of the 100 m photic zone in 1.23 days. This relative similarity of particle sedimentation rates for freshwater and saltwater was shown, specifically where the settling
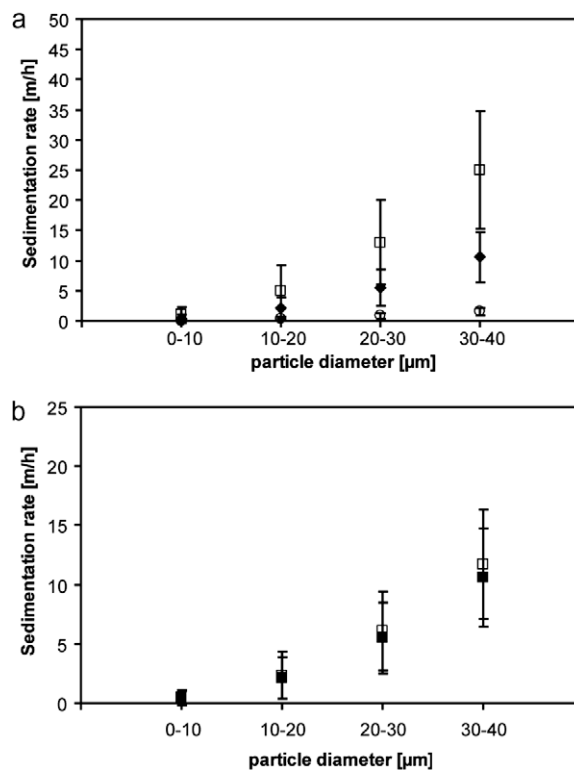

Fig. 7. Sedimentation rates calculated from measured particle sizes and density. (a) Sedimentation rates of cell–mineral aggregates produced by *Rhodobacter ferrooxidans* sp. strain SW2 grown on Fe(II) (◆), abiogenic ferrihydrite (□) and *Rhodobacter ferrooxidans* cells alone (○) as calculated for seawater. (b) The sedimentation rates calculated for cell–mineral aggregates produced by *Rhodobacter ferrooxidans* sp. strain SW2 grown on Fe(II) in seawater (■) as compared to freshwater (□) using the same data used for (a).

velocity of lake snow was reported to be fairly similar to marine snow (Grossart and Simon, 1993).

3.3. Mineral transformation and diagenesis of aggregates

The organic component of the cell–Fe mineral aggregates will determine surface charge, but also drive secondary abiotic and biotic mineral transformation processes. As most organic carbon is recycled in the water column and in the unconsolidated sediment, this makes these particles highly reactive during precipitation and the early stages of sediment diagenesis.

While the poorly crystalline Fe phases can remain stable for years when dried, they eventually transform into hematite (via dehydration), goethite and lepidocrocite (through Fe(II) catalyzed transformation) in aqueous suspension, depending on pH and solution chemistry (Schwertmann and Cornell, 2000). In lab experiments, and dependent upon solution chemistry and presence of nucleation sites, the initially formed Fe(III) mineral precipitated by the anoxygenic phototroph *R. ferrooxidans* sp. strain SW2 (poorly crystalline ferric hydroxide) converts to the more crystalline goethite and lepidocrocite after approximately

one month (Kappler and Newman, 2004). This transition is potentially stimulated by the presence of small amounts of remaining Fe(II) in solution or by slow microbially catalyzed Fe(III) reduction (Hansel et al., 2003; Kappler and Newman, 2004).

The rates of chemical and microbial iron (III) mineral transformation depend on mineral surface properties, such as the presence of sorbed Fe(II), the point of zero charge (ZPC) and the number of available reactive surface sites (i.e., the surface area) (Roden and Zachara, 1996; Roden, 2003). The bioavailable mineral surface is inversely dependent on crystallinity, and mineral aggregate size. As iron minerals with different crystal sizes vary significantly in surface area, they have varying stability, solubility and reactivity (Schwertmann and Cornell, 2000). BET analysis of chemically synthesized ferrihydrite yielded values of between 250 and 350 m^2/g (Cornell and Schwertmann, 2003). Recent studies of poorly crystalline biogenic minerals produced by the Fe(II)-oxidizing anaerobe *Acidovorax* sp. strain BoFeN1 showed BET of 158 m^2/g. Yet, aside from surface area, microbial mineral transformation rates have also been found to be controlled by Fe(III) oxide solubility, as has been tested for microbial Fe(III) reduction (Bonneville et al., 2004). As mentioned earlier, the primary mineral product of carbonate buffered microbial Fe(II) oxidation studied herein transformed either to goethite ($K_{sp} = 1 \times 10^{-41}$) in systems of low phosphate or Fe(III) phosphate ($K_{sp} = 1 \times 10^{-26}$) in systems of higher phosphate, so that in high phosphate systems microbial re-reduction may occur at higher rates (Bonneville et al., 2004).

In modern aqueous environments where Fe(II) is present, the small (<100 μm) cell–Fe(III) mineral aggregates help contribute to the downward sediment flux, but as was evident from the present experiments, a fraction of cells always remained planktonic at the end of Fe(II) oxidation; the consequence being a constant stoichiometric excess of Fe(III) in the precipitate. The fraction of organic carbon present, and the stoichiometric excess of Fe(III) shown by these experiments, could help drive Fe(III) re-reduction and Fe(II) remobilization (Konhauser et al., 2005). Stemming from this cycle, Fe(II) would also be provided as an energy rich substrate for chemolithotrophic microorganisms. Short- and long-term diagenesis transformations, driven respectively by microbial reduction and temperature and pressure, would incorporate any metals or ionic species sorbed to the falling aggregate and may even influence fossil or biomarker preservation.

3.4. The relevance of cell–mineral aggregates for BIF deposition in ancient environments

Given the probable antiquity of anoxygenic Fe(II)-oxidizing phototrophs (Widdel et al., 1993; Papineau et al., 2005; Xiong, 2006; Rashby et al., 2007), the identity, size, density and composition of modern analog cell–mineral aggregates may tell us more about the characteristic processes in early ocean water columns and sediments. These

organisms have been proposed as key players in the deposition of ancient iron deposits known as banded iron formations (BIF) (Konhauser et al., 2002; Posth et al., 2008), which are studied today as geological archives of past climate and biosphere (Konhauser et al., 2009). As Precambrian oceans were characterized by a high Fe flux, high silica concentrations (up to 2 mM as compared to the 70 μM average for modern oceans), a circumneutral pH (Grotzinger and Kasting, 1993) and anoxic conditions, which allowed the iron to accumulate (Holland, 1973; Anbar et al., 2007), biogenic Fe minerals likely constituted a significant fraction of the pelagic sediment in the ancient oceans.

In an ancient ocean basin in which BIF precipitated, very little carbon is found (<0.5%; Gole and Klein, 1981) which in the past seemed to negate the possibility of a microbial mechanism, such as proposed by the anoxygenic phototroph model. As shown in Eq. (1), anoxygenic Fe(II)-oxidizing phototrophy theoretically yields a molar ratio of 4Fe:1C. Accordingly, 90.0 mol Fe(III) m^{-2} $year^{-1}$ produced annually by anoxygenic phototrophs in a basin the size of the Hamersley would correspond to $\frac{1}{4}$ that amount in C, or 22.5 mol m^{-2} (2.3×10^{12} mol C for the entire range) (Konhauser et al., 2005). However, in the present study, a constant stoichiometric excess of Fe(III) was found in the precipitate after the completion of Fe(II) oxidation. This excess of Fe(III) may explain the lack of high amounts of C expected if a microbial process were to have played a role in BIF deposition. The BIF carbon record was likely influenced by the microbial processes active in the depositional basin, as well as any transformation pathways acting on the cell–mineral aggregate precipitate. Through processes such as fermentation to H_2 or methanogenesis to CH_4, the reactivity of the cell–mineral aggregate could promote conversion of complex compounds in both the water column and seafloor sediment and remove electrons from the system that would allow Fe(III) reduction. As a comparison, it is known that organic matter–cell aggregates (marine snow) are sites of enhanced microbial activity; the decomposition of which is also a source of considerable nutrient release into the water column (Wakeman and Lee, 1993). These organic matter–cell aggregates in lake systems even comprise anoxic microzones which can support anaerobic processes within an oxic water body (Paerl and Prufert, 1987).

The excess of Fe(III) minerals to C in BIF sediments may also have stemmed from an additional microbial Fe(II) oxidation mechanism, which would shift the Fe:C ratio (Konhauser et al., 2005). For example, either aerobic microbial Fe(II) oxidation without the deposition of the biomass produced in this process or, alternatively, aerobic, abiotic Fe(II) oxidation via cyanobacterial oxygen without the precipitation of the cyanobacterial biomass could both lead to an excess of Fe(III) in the deposits. Yet, as shown in this study, a stoichiometric excess of Fe(III) is also possible with a photoferrotrophic mechanism and would lead to a reduced amount of carbon in the sediment. It is furthermore conceivable that if photoferrotrophs remain planktonic or are converted in the water column, the majority

of Fe(III) turnover in an ancient basin sediment could be driven by Fe(III)-reducing bacteria (Johnson et al., 2008; Wu et al., 2009). Konhauser et al. (2005) estimated how much Fe(III) produced via anoxygenic phototrophs was found again in BIF deposits and conclude that with this depositional mechanism, as much as 70% could have been recycled back into the water column. Indeed, while the average oxidation state of $Fe^{+2.4}$ in BIF could be explained by the simultaneous deposition of Fe(II) and Fe(III), the partial microbial reduction of Fe(III) to Fe(II) could have also caused this mixed oxidation state.

The organic carbon present in the sediment via any of these microbial mechanisms would additionally drive mineral transformations under temperature and pressure conditions over geological time. In the anoxic setting of the BIF basin, any fermentation products in the shallow sediments would have been oxidized via some form of anaerobic respiratory process (Rothman et al., 2003). Minimal nitrate and sulfate would be available due to the lack of O_2 (Ewers and Morris, 1981; Strauss, 2003). The presence of MnO_2 was likely not significant as the concentration of Mn(II) released in hydrothermal effluent is up to 5 times lower than that of iron (Campbell et al., 1988) and there are presently no known anoxygenic phototrophic Mn(II)-oxidizing bacteria which would attest the importance of this pathway. However, the ferric hydroxide in a BIF depositional basin, as well as the partially reduced phases such as magnetite found in BIF could have supported a microbial process coupling the oxidation of organic carbon to the reduction of ferric iron (Nealson and Myers, 1990; Johnson et al., 2008).

Recently, Kappler et al. (2005a) estimated that in an area as large as the Hamersley (1×10^{11} m^2), it would only require a 17.6-m thick layer of anoxygenic Fe(II)-oxidizing phototrophic *R. ferrooxidans* sp. strain SW2 cells growing at least at 100 m depth below a wind-mixed ocean surface layer to generate 9.0×10^{12} mol Fe(III) annually or 90.0 mol Fe(III) m^{-2} year^{-1}. Accordingly, considering the 20 μm average particle size established for the anoxygenic phototroph biogenic minerals in this study, it would require approximately 3.4 days for such a particle to fall 400 m through seawater to the basin floor. As we have seen from these experiments using the modern analog bacteria, not all of the cells are dragged out of solution as part of the aggregate. This means that some cells could have remained in the water column continuing Fe(II) oxidation phototrophically.

4. SUMMARY AND CONCLUSIONS

Anoxygenic photosynthetic Fe(II)-oxidizing bacteria produce small (<100 μm), bulbous or ragged aggregates, with high surface areas that are highly reactive. In the presence of high concentrations of phosphate and Fe(II) min-eral phases, poorly ordered ferrihydrite is formed, whereas strains cultured in dissolved Fe(II) medium and lowered concentrations of phosphate produced goethite. These variations demonstrate how the solution chemistry influences mineral product identity. Cell–mineral aggregate size was shown to be primarily driven by cell aggregation behavior and cell size, rather than the presence of higher initial Fe(II) concentrations. Cell–mineral aggregate density ranged between 2.0 and 2.4 g/cm^3, with a small fraction higher than 2.4 g/cm^3. These low densities can be attributed to the organic carbon (cell) component of these aggregates, as chemically synthesized Fe(III) minerals, such as goethite, magnetite, lepidocrocite and ferrihydrite, have higher densities. Studies of cell–mineral co-precipitation and aggregate composition showed that the organic carbon (cell) fraction in the precipitate increases greatly with an increase in initial Fe(II) concentration. Notably, in all experiments, a fraction of the cells remained planktonic, demonstrating a constant stoichiometric excess of Fe(III) in the precipitate, which has implications for understanding sediment–water interface reactions in both ancient and modern settings. For example, sorption to these minerals would have consequences for sediment porosity, but also for flow and pollutant transport modeling and remediation. For studies of ancient settings, the long-term temperature and pressure driven diagenetic fate of the carbon and the iron in the cell–mineral aggregates could be tested in order to determine the potential for preservation.

APPENDIX. .

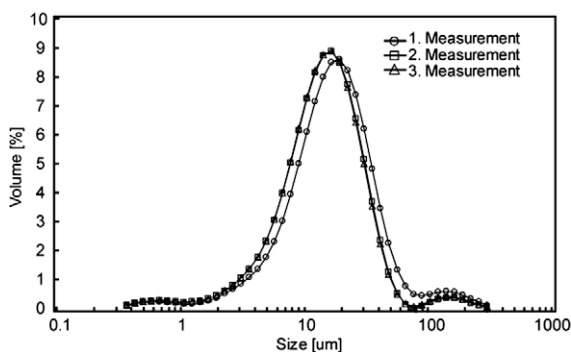See Fig. A1, Fig. A2, Table A1, Table A2, Fig. A3, Fig. A4.

Fig. A1. Particle size distribution shift to slightly smaller particle sizes in the second and third measurements of the same sample, suggesting mechanical disintegration during circulation/pumping of the particle suspension through the measuring chamber in the instrument.
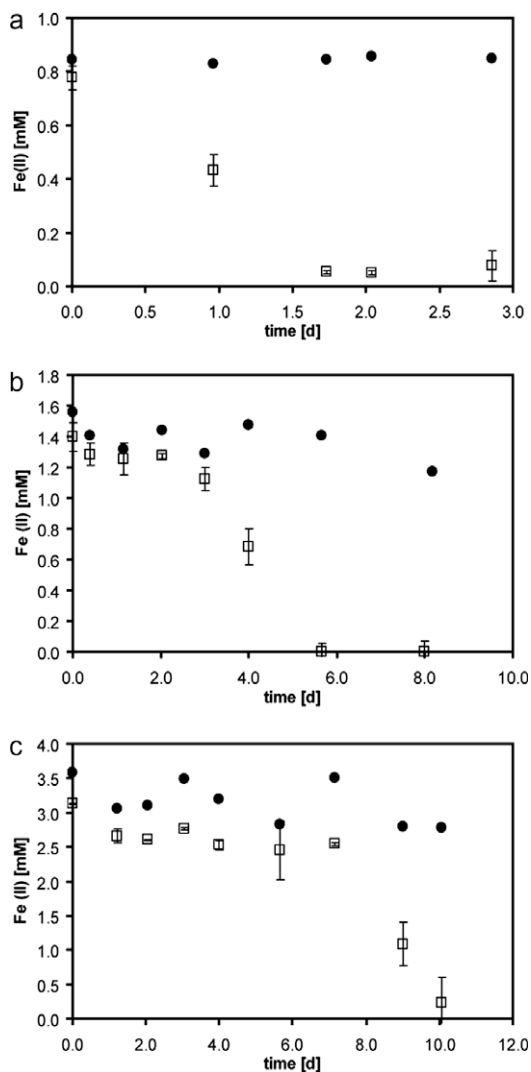

Fig. A2. The Fe(II) oxidation of (a) 0.8 mM, (b) 2 mM and (c) 4 mM starting Fe(II) concentrations by anoxygenic phototroph *Rhodobacter ferrooxidans* sp. strain SW2 for experiments in which cell counts were also analyzed. Abiotic blanks (●) are compared to triplicates of Fe(II) oxidation in microbial set-ups (□).

Table A1

Ions present in bacterial growth medium used in these studies. The freshwater growth medium used for the cultivation of Fe(II)-oxidizing phototrophs in the laboratory medium is modified from (Ehrenreich and Widdel, 1994). It contains 0.6 g/l potassium phosphate (KH$_2$PO$_4$), 0.3 g/l ammonium chloride (NH$_4$Cl); 0.5 g/l magnesium sulfate (MgSO$_4$·7H$_2$O) and 0.1 g/l calcium chloride (CaCl$_2$·2H$_2$O). The medium is buffered to pH 6.8–6.9 with 22 mmol/l bicarbonate. After autoclaving, 1 ml/l trace element solution (Tschech and Pfennig, 1984), 1 ml/l selenate–tungstate solution (Widdel, 1980) and 1 ml/l sterile filtered vitamin solution (Widdel and Pfennig, 1981) are added. For details on medium preparation, see Hegler et al. (2008).

	mol/l
Ion	
K$^+$	0.00440
H$_2$PO$_4^-$	0.00440
HPO$_4^{2-}$	0.00440
NH$_4^+$	0.00560
Cl$^-$	0.00560
Mg^{2+}	0.00200
SO$_4^{2-}$	0.00200
Ca^{2+}	0.00067
HCO$_3^-$	0.02200
Vitamins	
4-Aminobenzoic acid	0.000000360
D(+) biotin	0.000000041
Nicotinic acid	0.000081000
Ca-D(+) pantothenate	0.000000110
Pyridoxamine (Vit. B6) dihydrochloride	0.000001030
Thiaminium (Vit. B1) dihydrochloride	0.000000150
Cyanocobalamin	0.000000150
Trace elements	
25% HCl	10 ml/l
FeCl$_2$·4H$_2$O	1.5 g/l
H$_3$BO$_3$	30 mg
MnCl$_2$·4H$_2$O	100 mg
CoCl$_2$·6H$_2$O	190 mg
NiCl$_2$·6H$_2$O	24 mg
CuCl$_2$·2H$_2$O	2 mg
ZnCl$_2$	70 mg
Na$_2$MoO$_4$·2H$_2$O	36 mg
Se–W solution	
NaOH	0.4 g/l
Na$_2$SeO$_3$·5H$_2$O	6 mg
Na$_2$WO$_4$·2H$_2$O	8 mg

Table A2
Estimation of the Fe/C ratio in cell–mineral aggregates at the end of Fe(II) oxidation produced by anoxygenic phototrophic bacteria *Rhodobacter ferrooxidans* sp. strain SW2. Initial Fe(II) concentration of 0.8, 2.0 and 4.0 mM. These values correspond to both Fig. 3 and Table 2.

Initial Fe(II) concentration (mM)	mmol/l	mol/l	g Fe/l	mg Fe/l
Total Fe in the cell–mineral aggregates at the end of Fe(II) oxidation				
0.8	0.74	0.000740	0.0414	41.44
2.0	1.80	0.001800	0.1008	100.80
4.0	3.71	0.003710	0.2078	207.76

Initial Fe(II) concentration (mM)	Total cells in aggregate	mg C/l
Cells in the cell–mineral aggregates at the end of Fe(II) oxidation		
0.8	2.3×10^8	23
2.0	2.3×10^8	23
4.0	9.3×10^8	9.3

Important values: dry weight of cells based on the dry weight in early stationary phase (*Escherichia coli*), 200 fg (Loferer-Krössbacher et al., 1998). The percent of dry mass that is carbon, 50% (Neidhardt et al., 1990). Resulting dry weight in C considered here was 100 fg (1×10^{-10} mg).

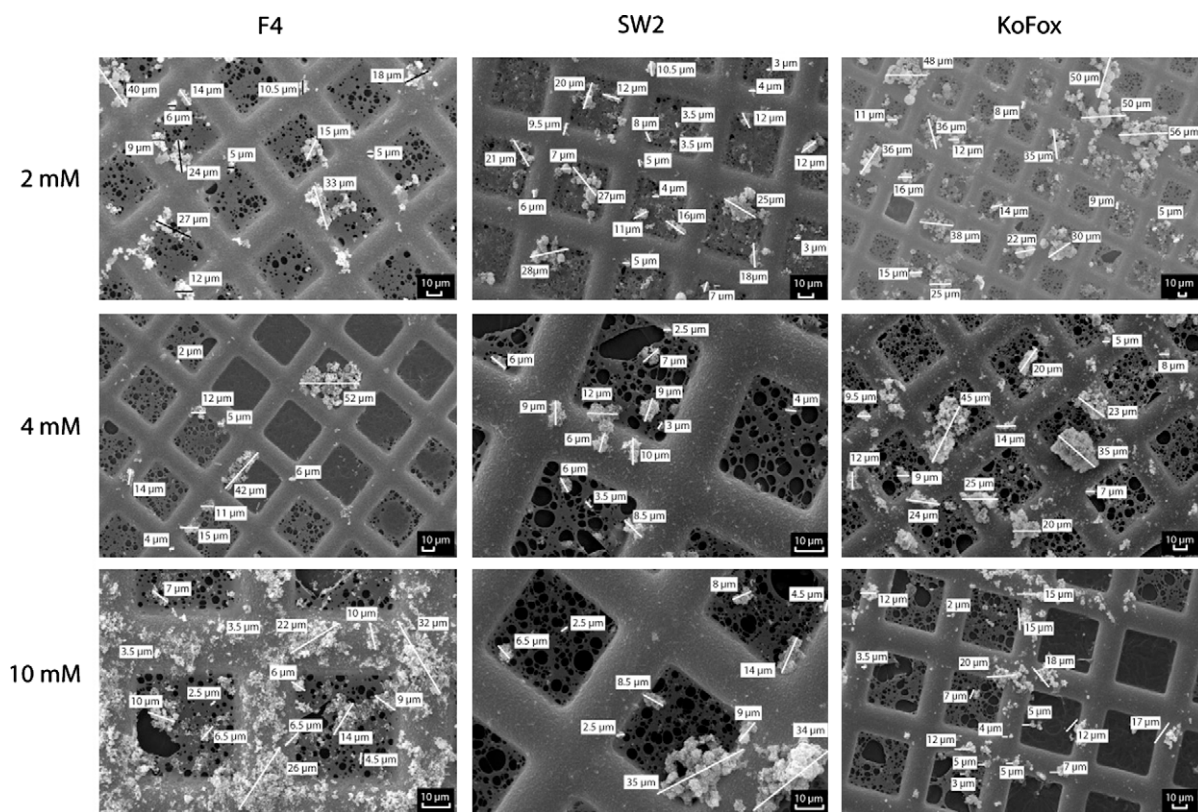| Initial Fe(II) concentration (mM)	mg Fe/l	mg C/l	Fe/C
Ratio of Fe/C in the aggregates			
0.8	41.44	2.30×10^{-1}	1.80
2	100.80	2.30×10^{-1}	4.38
4	207.76	9.28×10^{-1}	2.24

Fig. A3. Scanning electron micrographs of cell–mineral aggregates produced by *Thiodictyon* sp. strain F4, *Rhodobacter ferrooxidans* sp. strain SW2 and *Chlorobium ferrooxidans* sp. strain KoFox by the oxidation of 2, 4 and 10 mM Fe(II). Images illustrate data provided in Table 2.
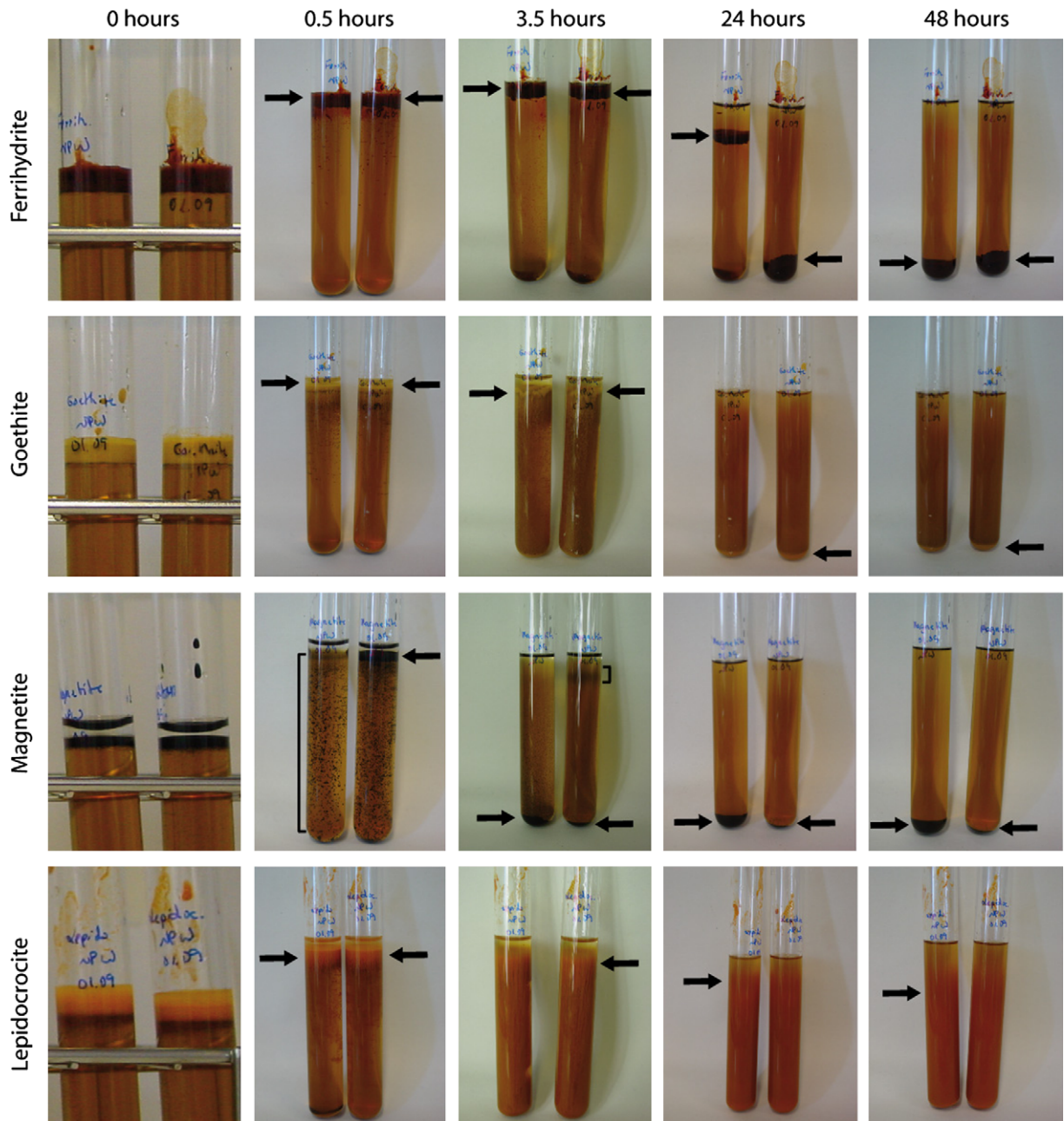
Fig. A4. Sedimentation of goethite, lepidocrocite, magnetite and ferrihydrite in sodium polytungstate solutions set to a density of 3.01 g/cm^3. Sedimentation of these chemically synthesized iron minerals shown at time 0 and at 0.5, 3.5, 24 and 48 h after the addition of the samples to the solution. Parallels are shown for each iron (oxy)hydroxide. Arrows and bars show where the precipitates were visible at each time point.

REFERENCES

Anbar A. D., Duan Y., Lyons T. W., Arnold G. L., Kendall B., Creaser R. A., Kaufman A. J., Gordon G. W., Scott C., Garvin J. and Buick R. (2007) A whiff of oxygen before the great oxidation event?. *Science* **317** 1903–1906.

Bonneville S., Van Cappellen P. and Behrends T. (2004) Microbial reduction of iron (III) oxyhydroxides: effects of mineral solubility and availability. *Chem. Geol.* **212**, 255–268.

Brocks J. J., Love G. D., Summons R. E., Knoll A. H., Logan G. A. and Bowden S. A. (2005) Biomarker evidence for green and purple sulphur bacteria in a stratified Palaeoproterozoic sea. *Nature* **437**, 866–870.

Brown D. A., Sherriff B. L., Sawicki J. A. and Sparling R. (1999) Precipitation of iron minerals by a natural microbial consortium. *Geochim. Cosmochim. Acta* **63**(15), 2163–2169.

Campbell A. C., Palmer M. R., Klinkhammer G. P., Bowers T. S., Edmond J. M., Lawrence J. R., Casey J. F., Thompson G., Humphris S., Rona P. and Karson J. A. (1988) Chemistry of hot springs on the Mid-Atlantic Ridge. *Nature* **335**, 514–519.

Canfield D. E. (1989) Reactive iron in marine sediments. *Geochim. Cosmochim. Acta* **53**, 619–632.

Chatellier X., Fortin D., West M. M., Rose J., Leppard G. G. and Ferris F. G. (2001) Effect of the presence of bacterial surfaces during the synthesis of Fe oxides by oxidation of ferrous ions. *Eur. J. Mineral.* **13**, 705–714.

Chatellier X., West M. M., Rose J., Fortin D., Leppard G. G. and Ferris F. G. (2004) Characterization of iron-oxides formed by oxidation of ferrous iron in the presence of various bacterial species and inorganic ligands. *Geomicrobiol. J.* **21**, 99–112.

Clarke W. A., Konhauser K. O., Thomas J. C. and Bottrell S. H. (1997) Ferric hydroxide and ferric hydroxysulfate precipitation by bacteria in an acid mine drainage lagoon. *FEMS Microbiol. Rev.* **20**, 351–361.

Cornell R. and Schwertmann U. (2003) *The Iron Oxides: Structures, Properties, Reactions, Occurrences and Uses*, second ed. Wiley-VCH, Weinheim.

Croal L., Johnson C., Beard B. and Newman D. (2004) Iron isotope fractionation by Fe(II)-oxidizing photoautotrophic bacteria. *Geochim. Cosmochim. Acta* **68**(6), 1227–1242.

Croal L. R., Jiao Y. and Newman D. K. (2007) The fox operon from *Rhodobacter* strain SW2 promotes phototrophic Fe(II) oxidation in *Rhodobacter capsulatus* SB1003. *J. Bacteriol.* **189**(5), 1774–1782.

Ehrenreich A. and Widdel F. (1994) Anaerobic oxidation of ferrous iron by purple bacteria, a new type of phototrophic metabolism. *Appl. Environ. Microbiol.* **60**(12), 4517–4526.

Ewers W. E. and Morris R. C. (1981) Studies of the Dales Gorge Member of the Brockman iron formation, Western Australia. *Econ. Geol.* **76**, 1929–1953.

Ferris F. G. (2005) Biogeochemical properties of bacteriogenic iron oxides. *Geomicrobiol. J.* **22**, 79–85.

Fortin D., Leppard G. G. and Tessier A. (1993) Characteristics of lacustrine diagenetic iron oxyhydroxides. *Geochim. Cosmochim. Acta* **57**, 4391–4404.

Fortin D. and Langley S. (2005) Formation and occurrence of biogenic iron-rich minerals. *Earth Sci. Rev.* **72**, 1–19.

Garrels R. M., Perry, Jr., E. A. and MacKenzie F. T. (1973) Genesis of Precambrian iron-formations and the development of atmospheric oxygen. *Econ. Geol.* **68**, 1173–1179.

Glasrud G. G., Navarette R. C., Scriven L. E. and Macosko C. (1993) Settling behaviors if iron oxide suspensions. *AIChE J.* **39**, 560–568.

Gole M. J. and Klein C. (1981) Banded iron formations through much of Precambrian time. *J. Geol.* **89**, 169–183.

Grossart H.-P. and Simon M. (1993) Limnetic macroscopic organic aggregates (lake snow): occurence, characteristics, and microbial dynamics in Lake Constance. *Limnol. Oceanogr.* **38**(3), 532–546.

Grotzinger J. P. and Kasting J. F. (1993) New constraints on Precambrian ocean composition. *J. Geol.* **101**, 235–243.

Hansel C. M., Benner S. G., Neiss J., Dohnalkova A., Kukkadapu R. K. and Fendorf S. (2003) Secondary mineralization pathways induced by dissimilatory iron reduction of ferrihydrite under advective flow. *Geochim. Cosmochim. Acta* **67**(16), 2977–2992.

Hansel C. M., Benner S. G., Nico P. and Fendorf S. (2004) Structural constraints of ferric (hydr)oxides on dissimilatory iron reduction and the fate of Fe(II). *Geochim. Cosmochim. Acta* **68**(15), 3217–3229.

Hartman H. (1984) The evolution of photosynthesis and microbial mats: a speculation on banded iron formations. In *Microbial Mats: Stromatolites* (eds. Y. Cohen, R. W. Castenholz and H. O. Halvorson). Alan Liss, New York, pp. 451–453.

Hegler F., Posth N. R., Jiang J. and Kappler A. (2008) Physiology of phototrophic iron(II)-oxidizing bacteria: implications for modern and ancient environments. *FEMS Microbiol. Ecol.* **66**, 250–260.

Heising S. and Schink B. (1998) Phototrophic oxidation of ferrous iron by a *Rhodomicrobium vannielii* strain. *Microbiology* **144**, 2263–2269.

Heising S., Richter L., Ludwig W. and Schink B. (1999) *Chlorobium ferrooxidans* sp. nov., a phototrophic green sulfur bacterium that oxidizes ferrous iron in coculture with a *Geospirillum* sp. strain. *Arch. Microbiol.* **172**, 116–124.

Hohmann C., Winkler E., Morin G. and Kappler A. (2010) Anaerobic Fe(II)-oxidizing bacteria show As resistance and coprecipitate As during Fe(III) mineral precipitation. *Environ. Sci. Technol.* **44**, 94–101.

Holland H. D. (1973) The oceans: a possible source of iron in iron-formations. *Econ. Geol.* **68**, 1169–1172.

James R. E. and Ferris F. G. (2004) Evidence for microbial-mediated iron oxidation at a neutrophilic groundwater spring. *Chem. Geol.* **212**, 301–311.

Jiao Y. and Newman D. K. (2007) The pio operon is essential for phototrophic Fe(II) oxidation in *Rhodopseudomonas palustris* TIE-1. *J. Bacteriol.* **189**(5), 1765–1773.

Johnson C., Beard B. L. and Roden E. E. (2008) The iron isotope fingerprints of redox and biogeochemical cycling in modern and ancient earth. *Annu. Rev. Earth Planet. Sci.* **36**, 457–493.

Kappler A. and Newman D. K. (2004) Formation of Fe (III) minerals by Fe(II) oxidizing photoautotrophic bacteria. *Geochim. Cosmochim. Acta* **68**(6), 1217–1226.

Kappler A. and Straub K. L. (2005) Geomicrobiological cycling of iron. *Rev. Mineral. Geochem.* **59**, 85–108.

Kappler A., Pasquero C., Konhauser K. O. and Newman D. K. (2005a) Deposition of banded iron formations by anoxygenic phototrophic Fe(II)-oxidizing bacteria. *Geology* **33**, 865–868.

Kappler A., Schink B. and Newman D. K. (2005b) Fe(III) mineral formation and cell encrustation by the nitrate-dependent Fe(II) oxidizer strain BoFeN1. *Geobiology* **3**, 235–245.

Konhauser K. (1997) Bacterial biomineralization in nature. *FEMS Microbiol. Rev.* **20**, 315–326.

Konhauser K., Hamade T., Raiswell R., Morris R. C., Ferris F. G., Southam G. and Canfield D. E. (2002) Could bacteria have formed the Precambrian banded iron formations? *Geology* **30**, 1079–1082.

Konhauser K., Newman D. K. and Kappler A. (2005) The potential significance of microbial Fe(III) reduction during deposition of Precambrian banded iron formations. *Geobiology* **3**, 167–177.

Konhauser K. O., Pecoits E., Lalonde S. V., Papineau D., Nisbet E. G., Barley M. A., Arndt N. T., Zahnle K. and Kamber B. S. (2009) Oceanic nickel depletion and a methanogen famine before the great oxidation event. *Nature* **458**, 750–753.

Langley S., Gault A., Ibrahim A., Renaud R., Fortin D., Clark I. D. and Ferris F. G. (2009) A comparison of the rates of Fe(III) reduction in synthetic and bacteriogenic iron oxides by *Shewanella putrefaciens* CN32. *Geomicrobiol. J.* **26**, 57–70.

Loferer-Krössbacher M., Klima J. and Psenner R. (1998) Determination of bacterial cell dry mass by transmission electron microscopy and densitometric image analysis. *Appl. Environ. Microbiol.* **64**(2), 688–694.

Lovley D. R. and Phillips E. J. P. (1986) Availability of ferric iron for microbial reduction in bottom sediments of the freshwater tidal Potomac River. *Appl. Environ. Microbiol.* **52**, 751–757.

Miot J., Benzerara K., Morin G., Kappler A., Bernard S., Obst M., Férard C., Skouri-Panet F., Guigner J.-M., Posth N. R., Galvez M., Brown, Jr., G. E. and Guyot F. (2009) Iron biomineralization by anaerobic neutrophilic iron-oxidizing bacteria. *Geochim. Cosmochim. Acta* **73**, 696–711.

Nealson K. H. and Myers C. R. (1990) Iron reduction by bacteria: a potential role in the genesis of banded iron formations. *Am. J. Sci.* **290-A**, 35–45.

Neidhardt F., Ingraham J. and Schaechter M. (1990) *Physiology of the Bacterial Cell: A Molecular Approach*. Sinauer Associates, Inc., Sunderland, Massachusetts.

Paerl H. W. and Prufert L. E. (1987) Oxygen-poor microzones as potential sites of microbial N2 fixation in nitrogen-depleted aerobic marine waters. *Appl. Environ. Microbiol.* **53**(5), 1078–1087.

Papineau D., Walker J. J., Mojzsis S. J. and Pace N. R. (2005) Composition and structure of microbial communities from stromatolites of Hamelin pool in Shark Bay, Western Australia. *Appl. Environ. Microbiol.* **71**, 4822–4832.

Posth N. R., Hegler F., Konhauser K. O. and Kappler A. (2008) Alternating Si and Fe deposition caused by temperature fluctuations in Precambrian oceans. *Nat. Geosci.* **1**(10), 703–708.

Posth N. R., Konhauser K. O. and Kappler A. (in press) Microbiological processes in BIF deposition. In Authigenic Minerals: Sedimentology, Geochemistry, Origins, Distribution and Applications, *J. Sedimentology IAS Special Publication Series* (eds. C. Glenn and I. Jarvis).

Postma D. (1993) The reactivity of iron oxides in sediments: a kinetic approach. *Geochim. Cosmochim. Acta* **57**, 5027–5034.

Rashby S. E., Sessions A. L., Summons R. E. and Newman D. K. (2007) Biosynthesis of 2-methylbacteriohopanepolyols by an anoxygenic phototroph. *Proc. Natl. Acad. Sci. USA* **104**, 15099–15104.

Roden E. (2003) Fe(III) oxide reactivity toward biological versus chemical reduction. *Environ. Sci. Technol.* **37**, 1319–1324.

Roden E. (2004) Analysis of long-term bacterial vs. chemical Fe(III) oxide reduction kinetics. *Geochim. Cosmochim. Acta* **68**(15), 3205–3216.

Roden E. and Zachara J. (1996) Microbial reduction of crystalline iron (III) oxides: influence of oxid surface area and potential for cell growth. *Environ. Sci. Technol.* **30**, 1618–1628.

Rothman D. H., Hayes J. M. and Summons R. E. (2003) Dynamics of the Neoproterozoic carbon cycle. *Proc. Natl. Acad. Sci. USA* **100**, 8124–8129.

Schädler S., Burkhardt C. and Kappler A. (2008) Evaluation of electron microscopic sample preparation methods and imaging techniques for characterization of cell–mineral aggregates. *Geomicrobiol. J.* **25**, 228–239.

Schädler S., Burkhardt C., Hegler F., Straub K. L., Miot J., Benzerara K. and Kappler A. (2009) Formation of cell–iron–mineral aggregates by phototrophic and nitrate-reducing anaerobic Fe(II)-oxidizing bacteria. *Geomicrobiol. J.* **26**, 93–103.

Schwertman U., Friedl J. and Stanjek H. (1999) From Fe(III) ions to ferrihydrite and then to hematite. *J. Colloid Interface Sci.* **209**, 215–223.

Schwertmann U. and Cornell R. M. (2000) *Iron Oxides in the Laboratory*. Wiley-VCH, Weinheim.

Sobolev D. and Roden E. E. (2001) Suboxic deposition of ferric iron by bacteria in opposing gradients of Fe(II) and oxygen at circumneutral pH. *Appl. Environ. Microbiol.* **67**(3), 1328–1334.

Stookey L. (1970) Ferrozine—a new spectrophotometric reagent for iron. *Anal. Chem.* **42**, 779–781.

Straub K. L., Hanzlik M. and Buchholz-Cleven B. E. E. (1998) The use of biologically produced ferrihydrite for the isolation of novel iron-reducing bacteria. *Syst. Appl. Microbiol.* **21**, 442–449.

Strauss H. (2003) Sulphur isotopes and the early Archean sulphur cycle. *Precambrian Res.* **126**, 349–361.

Stumm W. and Morgan J. L. (1996) *Aquatic Chemistry: Chemical Equilibria and Rates in Natural Waters*. John Wiley & Sons, New York.

Suter D., Siffert C., Sulzberger B. and Stumm W. (1988) Catalytic dissolution of iron(III) (hydr)oxides by oxalic acid in the presence of Fe(II). *Naturwissenschaften* **75**, 571–573.

Thamdrup B. (2000) Bacterial manganese and iron reduction in aquatic sediments. *Adv. Microb. Ecol.* **16**, 41–84.

Trouwborst R. E., Johnston A., Koch G., Luther, III, G. W. and Pierson B. K. (2007) Biogeochemistry of Fe(II) oxidation in a photosynthetic microbial mat: implications for Precambrian Fe(II) oxidation. *Geochim. Cosmochim. Acta* **71**, 4629–4643.

Tschech A. and Pfennig N. (1984) Growth yield increase linked to caffeate reduction in *Acetobacterium woodii*. *Arch. Microbiol.* **137**, 163–167.

Viollier E., Inglett P., Hunter K., Roychoudhury A. and Van Cappellen P. (2000) The ferrozine method revisited: Fe(II)/Fe(III) determination in natural waters. *Appl. Geochem.* **15**, 785–790.

Wakeman S. G. and Lee C. (1993) Production, transport, and alteration of particulate organic matter in the marine water column. In *Organic Geochemistry* (eds. M. H. Engel and S. A. Macko). Plenum Press, New York, pp. 145–169.

Weber K. A., Achenbach L. A. and Coates J. D. (2006) Microorganisms pumping iron: anaerobic microbial iron oxidation and reduction. *Nat. Rev.* **4**, 752–764.

Widdel F. (1980) Anaerober Abbau von Fettsäuren und Benzoesäure durch neu isolierte Arten Sulfat-reduzierender Bakterien. Doctorate dissertation, University of Göttingen, FRG.

Widdel F. and Pfennig N. (1981) Studies on dissimilatory sulfate-reducing bacteria that decompose fatty acids: I. Isolation of a new sulfate-reducer enriched with acetate from saline environments. Description of *Desulfobacter postgatei* gen. nov. sp. nov.. *Arch. Microbiol.* **129**, 395–400.

Widdel F., Schnell S., Heising S., Ehrenreich A., Assmus B. and Schink B. (1993) Ferrous iron oxidation by anoxygenic phototrophic bacteria. *Nature* **362**, 834–836.

Wu L., Beard B. L., Roden E. E. and Johnson C. M. (2009) Influence of pH and dissolved Si on Fe isotope fractionation during dissimilatory microbial reduction of hematite. *Geochem. Cosmochim. Acta* **73**, 5584–5599.

Yarzábal A., Brasseur G., Ratouchniak J., Lund K., Lemesle-Meunier D., DeMoss J. A. and Bonnefoy V. (2002) The high-molecular-weight cytochrome *c* Cyc2 of *Acidithiobacillus ferrooxidans* is an outer membrane protein. *J. Bacteriol.* **184**, 313–317.

Xiong J. (2006) Photosynthesis: What Color Was Its Origin? *Genome Biol.* **7**, 245.1–245.5.

Associate editor: Stephan M. Kraemer